Reprinted from

JAPANESE JOURNAL OF
APPLIED
PHYSICS

REGULAR PAPER

Increasing Bandwidth of Ultrasound Radio Frequency Echoes Using Wiener Filter for Improvement of Accuracy in Measurement of Intima–Media Thickness

Sho Kageyama, Hideyuki Hasegawa, and Hiroshi Kanai

Jpn. J. Appl. Phys. **52** (2013) 07HF04

Japanese Journal of Applied Physics **52** (2013) 07HF04 **REGULAR PAPER**
http://dx.doi.org/**10.7567/JJAP.52.07HF04**

Increasing Bandwidth of Ultrasound Radio Frequency Echoes Using Wiener Filter for Improvement of Accuracy in Measurement of Intima–Media Thickness

Sho Kageyama[1], Hideyuki Hasegawa[1,2], and Hiroshi Kanai[1,2]*

[1]*Graduate School of Biomedical Engineering, Tohoku University, Sendai 980-8579, Japan*
[2]*Graduate School of Engineering, Tohoku University, Sendai 980-8579, Japan*
E-mail: kanai@ecei.tohoku.ac.jp

Received November 21, 2012; revised December 27, 2012; accepted February 26, 2013; published online June 20, 2013

It is very important to make early diagnoses of atherosclerosis for the prevention of lifestyle-related diseases. The intima–media thickness (IMT) is used as a diagnostic index of cerebrovascular diseases and atherosclerosis throughout the body including the coronary artery. In the field of the medical diagnostics, ultrasonic equipment using a pulse–echo method is widely used. In conventional ultrasonic diagnostic equipment, ultrasonic images are obtained by receiving ultrasonic echoes and converting their amplitudes into brightness. In general, ultrasonic B-mode images are degraded by the narrow-band characteristics of the ultrasonic transducer. In the present study, a method was proposed for shortening the lengths of the received ultrasonic pulses from an object of interest using a Wiener filter. As a result, the lengths of ultrasonic pulses were shortened and the visibility of interfaces of the intima–media complex of the carotid arterial wall was improved by the proposed method, which realizes accurate measurement of the IMT.

1. Introduction

In recent years, cardiovascular diseases such as myocardial infarction have been increasing in Japan with the westernization of the diet, the aging of society, and a chronic lack of exercise due to modern lifestyles, which are the main causes of lifestyle-related diseases. It is very important to make early diagnoses of atherosclerosis for the prevention of these diseases. Ultrasonic diagnostic equipment has been widely used in clinical situations for various reasons including less physical and mental hardship to patients and non-invasiveness making it suitable for repetitive diagnosis in the early stages of diseases.

In the very early stages of atherosclerosis, it is known that the surface of the intima in the arterial wall becomes rough owing to insults to endothelial cells and the internal elastic lamina.[1)] Thus, the spatial resolution in the direction of the ultrasound beam should be comparable to the thickness of the endothelial cell in order to diagnose the surface roughness.[2)] In addition, the intima–media thickness (IMT) is used as a diagnostic index of atherosclerosis and cerebrovascular diseases throughout the body including the coronary artery.[3,4)]

In the field of medical diagnostics, ultrasonic diagnostic equipment using a pulse–echo method is widely used. In conventional ultrasonic diagnostic equipment, ultrasound images are obtained by receiving ultrasonic echoes and converting their amplitudes into brightness. There is a problem in the reconstructed images that affects clinical diagnosis. Ultrasonic images are degraded by a specific pattern called speckle noise. The speckle noise exhibits a pattern that occurs as a result of the random interference of ultrasonic echoes scattered in the living tissue, and the pattern might be misrecognized as nonuniformity of the living tissue due to its appearance. In general, an ultrasonic transducer used in ultrasonic diagnostic equipment has narrow-band characteristics. Therefore, the emitted ultrasonic pulses exhibit reverberation[5)] and, thus, the boundaries of the obtained images are blurred. For this reason, it is difficult to measure the IMT of the carotid arterial wall accurately, and it is difficult to diagnose atherosclerosis at an early stage. The accuracy of IMT measurement would be improved if the lengths of received ultrasonic pulses could be shortened, which means that the bandwidth of the received ultrasonic echo signal is broadened.

Methods have been developed for broadening the frequency characteristics of the received ultrasonic echoes to shorten the pulse length. These methods use spatial compounding[6–8)] and frequency compounding,[8–16)] resulting in improved spatial resolution. The spatial-compounding method is an image-synthesizing method that uses different images obtained by emitting ultrasound beams from different directions to the same region. The frequency-compounding method also synthesizes different images, which have different speckle patterns because ultrasonic signals with different center frequencies are used. However, the time resolution is degraded in the spatial-compounding method and the spatial resolution is degraded in the frequency-compounding method because images are compounded at different spatial resolutions.[8)] Moreover, in conventional ultrasonic transducers, it is known that speckle reduction using these compounding methods is not effective because they have narrow-band frequency characteristics.[17)]

In the present study, we focus on a filtering method using a Wiener filter[18–22)] as a method for shortening the lengths of the received ultrasonic pulses. Ideally, the received ultrasonic echoes are expressed as a convolution between the distribution of the scattering coefficients of objects, which have a wide-band characteristic, and the impulse response of the ultrasonic transducer (narrow band). The Wiener filter is designed as an inverse filter using the transfer characteristics of the transducer, which has narrow-band characteristics, and is weighted using the signal-to-noise ratio (SNR) to broaden the frequency characteristics of the transducer in the frequency range with a good SNR and also attenuate the power of the received echo signal in the frequency range with a low SNR. A received ultrasonic pulse is shortened by broadening its frequency characteristics using the Wiener filter.

2. Principles

2.1 Principle of Wiener filter $M_j(\omega)$

Figure 1 shows a block diagram illustrating how to estimate the spatial distribution of the reflectivity of an object $\hat{f}_{i,j}(t)$,

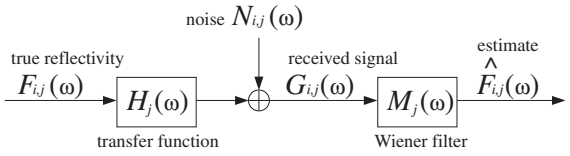

Fig. 1. Block diagram of the system for obtaining estimate $\hat{F}_{i,j}(\omega)$ using Wiener filter $M_j(\omega)$.

where $\hat{F}_{i,j}(\omega)$ is its frequency spectrum. In Fig. 1, $G_{i,j}(\omega)$, $H_j(\omega)$, $N_{i,j}(\omega)$, and $M_j(\omega)$ are the frequency spectra of the echo from an object, the transfer function of the transducer, noise, and the impulse response of the Wiener filter, respectively. In addition, i and j are the beam number and frame number, respectively. In the case of the measurement of an object with movement such as a carotid artery, the received echo varies frame by frame. Therefore, in the present study, the transfer function $H_j(\omega)$ and the Wiener filter $M_j(\omega)$ are estimated for each frame.

Wiener filter $M_j(\omega)$ is determined so as to minimize the mean squared difference between the spectrum of the true reflectivity $F_{i,j}(\omega)$ and its model $\hat{F}_{i,j}(\omega)$. The estimate $\hat{F}_{i,j}(\omega)$ is given by

$$\hat{F}_{i,j}(\omega) = G_{i,j}(\omega) \cdot M_j(\omega) = \frac{G_{i,j}(\omega) \cdot H_j^*(\omega)}{|H_j(\omega)|^2 + P_N(\omega)/P_F(\omega)}, \quad (1)$$

where $P_N(\omega)$ and $P_F(\omega)$ are the averaged power spectra of the noise and the true reflectivity $F_{i,j}(\omega)$, respectively.[18–22] However, the power spectrum $P_F(\omega)$ of the true signal $F_{i,j}(\omega)$ cannot be obtained, because the true reflectivity $F_{i,j}(\omega)$ is not obtained before applying the Wiener filter $M_j(\omega)$ to the received signal $G_{i,j}(\omega)$; thus, there is an inconsistency in the expression of the Wiener filter $M_j(\omega)$. Traditionally, for this problem, the power spectrum obtained by averaging the power spectra $[G_{i,j}(\omega)]$ is assumed as the power spectrum $P_F(\omega)$ of the true reflectivity.[4] However, $G_{i,j}(\omega)$ includes the transfer characteristics $H_j(\omega)$. Therefore, it is not appropriate to obtain the weighting function $P_N(\omega)/P_F(\omega)$ using the received ultrasonic echo $G_{i,j}(\omega)$. Therefore, we evaluated the SNR using the magnitude-squared coherence function (MSCF)[23] because $P_N(\omega)/P_F(\omega)$ is the inverse of the SNR. The MSCF $|\gamma_i(\omega)|^2$ is given by

$$|\gamma_i(\omega)|^2 = \frac{|E_j[G_{i,j}^*(\omega) \cdot G_{i,j+1}(\omega)]|^2}{E_j[|G_{i,j}^*(\omega)|^2] \cdot E_j[|G_{i,j+1}(\omega)|^2]}, \quad (2)$$

where $*$ is the complex conjugate. The MSCF $|\gamma_i(\omega)|^2$ is a function evaluating the phase coherency of echoes in different frames. Assuming that the noise is random, it is considered that the signal component has phase coherency and that the noise component is not coherent. Therefore, using the MSCF $|\gamma_i(\omega)|^2$, the SNR $W_{SNR}(\omega)$ is given by

$$W_{SNR}(\omega) = \frac{1}{N_{beam}} \sum_{i=0}^{N_{beam}-1} \frac{|\gamma_i(\omega)|^2}{1 - |\gamma_i(\omega)|^2}, \quad (3)$$

where N_{beam} is the number of beam positions.[23,24] Figure 2(a) shows an example of the MSCF and Fig. 2(b) shows the SNR, each of which was obtained by Eq. (3). We measured a silicone plate in water using a 10-MHz linear array probe (the sampling frequency of ultrasonic RF echoes was 40 MHz and the frame rate was 30 Hz). As shown in Fig. 2, ideally it is desirable for a transducer to have a wide bandwidth. However, the transducer used in measurement has narrow-band characteristics. As a result, the measured SNR also shows narrow-band characteristics. The Wiener filter, which applies weights to the frequency characteristics of the filter by considering the inverse of the SNR, operates as an inverse filter in the frequency range with a good SNR whereas the filter is suppressed in the frequency range with a low SNR. Therefore, the filter works in a very limited frequency band when the filter is directly weighted by the SNR.

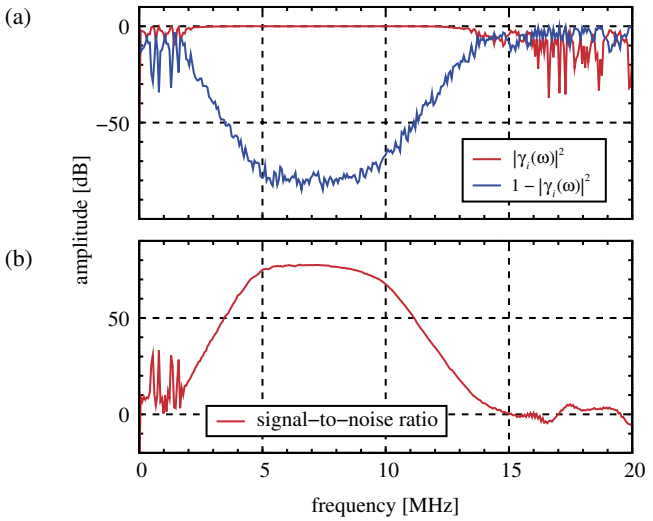

Fig. 2. (Color online) (a) Magnitude-squared coherence function $|\gamma_i(\omega)|^2$ and $1 - |\gamma_i(\omega)|^2$ ($i = 150$), (b) average signal-to-noise ratio $W_{SNR}(\omega)$ obtained using magnitude-squared coherence function $|\gamma_i(\omega)|^2$ in the measurement of a silicone plate at 13.5 mm depth in a water tank.

2.2 Identification of transfer function $H_j(\omega)$

2.2.1 Estimation of power of transfer function $H_j(\omega)$

The important issue in designing the Wiener filter is how to identify the transfer function $H_j(\omega)$. When image processing is carried out using the Wiener filter, $H_j(\omega)$ is commonly obtained from the point spread function (PSF).[25–27] The PSF can be obtained by measuring an echo from a point scatterer. This can be done by measuring a fine wire placed in a water tank. However, biological tissues exhibit frequency-dependent attenuation, which changes the waveform of an ultrasonic echo. Therefore, it is desirable to obtain the PSF from echoes from an object of interest. However, when an object has many point scatterers, there are many dips in the power spectrum of an echo signal due to interference, and such frequency characteristics cannot be used as the PSF.

In the transfer system shown in Fig. 1, $G_{i,j}(\omega)$ is the frequency spectrum of the echo signal obtained by ultrasound equipment. Assuming that $f_{i,j}(t)$ is the group of impulses, it is considered that $G_{i,j}(\omega)$ is the sum of $H_j(\omega)$ with different phase characteristics due to time delays of the impulses. The frequencies at which dips occur in the power spectrum $|G_{i,j}(\omega)|^2$ depend on the time delays of echoes. From this fact, frequencies with dips should be random from beam by beam due to the random distribution of scatterers in

tissue. Therefore, the power spectrum of the transfer function with noise $|H'_j(\omega)|^2$ is obtained by smoothing out the dips in $|G_{i,j}(\omega)|^2$ by averaging $\{|G_{i,j}(\omega)|^2\}$ obtained at different beam positions as follows:

$$\begin{aligned}|H'_j(\omega)|^2 &= \frac{1}{N_{\text{beam}}}\sum_{i=0}^{N_{\text{beam}}-1}|G_{i,j}(\omega)|^2 \\ &= \frac{1}{N_{\text{beam}}}\sum_{i=0}^{N_{\text{beam}}-1}|G'_{i,j}(\omega)+N_{i,j}(\omega)|^2 \\ &\approx \frac{1}{N_{\text{beam}}}\sum_{i=0}^{N_{\text{beam}}-1}(|G'_{i,j}(\omega)|^2+|N_{i,j}(\omega)|^2) \\ &= \frac{1}{N_{\text{beam}}}\sum_{i=0}^{N_{\text{beam}}-1}|G'_{i,j}(\omega)|^2\cdot\left(1+\frac{\sum_{i=0}^{N_{\text{beam}}-1}|N_{i,j}(\omega)|^2}{\sum_{i=0}^{N_{\text{beam}}-1}|G'_{i,j}(\omega)|^2}\right),\end{aligned} \tag{4}$$

where $G'_{i,j}(\omega)$ is the frequency spectrum of the received echo without noise $N_{i,j}(\omega)$. In Eq. (4), the terms $G'^{*}_{i,j}(\omega)\cdot N_{i,j}(\omega)$ and $G'_{i,j}(\omega)\cdot N^{*}_{i,j}(\omega)$ are assumed to become zero upon averaging because $G_{i,j}(\omega)$ and $N_{i,j}(\omega)$ are uncorrelated. To obtain $|H_j(\omega)|^2$ correctly, $|N_{i,j}(\omega)|^2$ must be removed from Eq. (4). In the present study, the power spectrum of noise $|N_{i,j}(\omega)|^2$ was estimated from the signal obtained during the measurement with no target in a water tank so that there was no echo (only noise is contained in the measured signal). The estimate of the power spectrum of noise $|\hat{N}_j(\omega)|^2$ was obtained by averaging the power spectra of the signal with no target measured at all beam positions. The power spectrum $|H_j(\omega)|^2$ of the transfer function is estimated by removing the estimated power spectrum of noise $|\hat{N}_j(\omega)|^2$ from that of the received echo $|G_{i,j}(\omega)|^2$ as follows:

$$\begin{aligned}|H_j(\omega)|^2 &= \frac{1}{N_{\text{beam}}}\sum_{i=0}^{N_{\text{beam}}-1}|G'_{i,j}(\omega)|^2 \\ &= \frac{1}{N_{\text{beam}}}\sum_{i=0}^{N_{\text{beam}}-1}(|G_{i,j}(\omega)|^2-|\hat{N}_j(\omega)|^2).\end{aligned} \tag{5}$$

The power spectrum of noise $|\hat{N}_j(\omega)|^2$ is shown in Fig. 3 with an example of the power spectrum of a received echo $|G_{i,j}(\omega)|^2$ measured in vivo. Ultrasonic echoes from the posterior wall of a carotid artery were measured in vivo and the reference power spectra at 5.0, 15.0, and 25.0 mm in the lateral direction ($i = 50$, 150, and 250, respectively) are shown in Fig. 4.

As shown in Fig. 4, some dips in the power spectra occurred at different frequencies owing to the interference of echoes from a large number of point scatterers. As a result, the phase of the ultrasonic RF echoes was different at different ultrasonic beam positions. The magnitude of the transfer function $|H_j(\omega)|$ estimated from the power spectra of the received echoes $|G_{i,j}(\omega)|^2$ using Eq. (5) is shown in Fig. 5, and $|G_{i,j}(\omega)|^2$ at 15.0 mm ($i = 150$, $j = 0$) in the lateral direction is also shown in the same figure. As shown in Fig. 5, some dips that occurred in $|G_{i,j}(\omega)|^2$ were suppressed by beam averaging, and the spectrum envelope was obtained. This spectrum envelope was used as the magnitude of the transfer function $|H_j(\omega)|$.

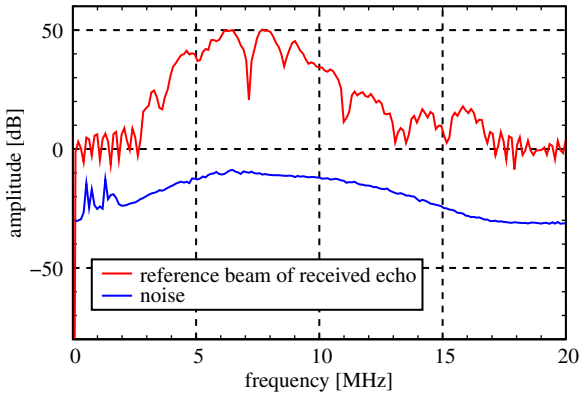

Fig. 3. (Color online) Power spectrum of the reference beam of the received echo $|G_{i,j}(\omega)|^2$ and that of noise $|\hat{N}_j(\omega)|^2$ obtained from the signal measured with no object in a water tank.

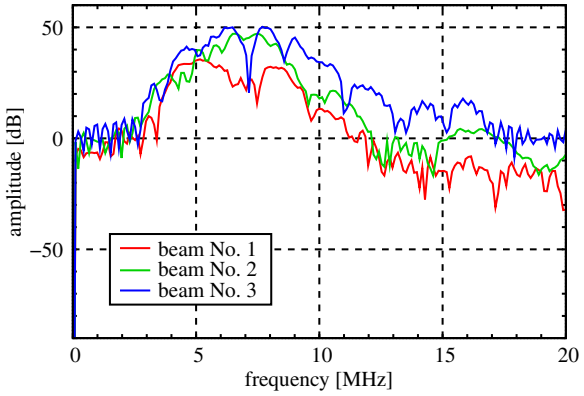

Fig. 4. (Color online) Generation of dips of the power spectra $\{|G_{i,j}(\omega)|^2\}$ in in vivo measurement at 5.0, 15.0, and 25.0 mm in the lateral direction ($i = 50$, 150, and 250, respectively).

2.2.2 Estimation of phase of transfer function $H_j(\omega)$

Section 2.2.1 proposed a method for estimating the magnitude $|H_j(\omega)|$ of a transfer function. However, as shown in Eq. (1), it is necessary to obtain the phase term of the transfer function. Therefore, this section describes a method for estimating the phase term of the transfer function.

In the present study, the magnitude $|H_j(\omega)|$ of the transfer function was estimated using ultrasonic echoes from an object of interest because $|H_j(\omega)|$ is influenced by the frequency-dependent attenuation of tissue. However, the phase $\angle H_j(\omega)$ should not be influenced by the attenuation of tissue. Therefore, in the present study, $\angle H_j(\omega)$ is obtained using the emitted ultrasonic pulse received by a hydrophone in a water tank. The signal $s(t)$ [whose frequency spectrum is denoted by $S(\omega)$] received by the hydrophone is composed of the frequency characteristics of the driving signal $X(\omega)$ and the transfer function of the ultrasonic transducer $Y_{\text{t}}(\omega)$. By assuming that the driving signal is an impulse, the phase $\angle H_j(\omega)$ of the transfer function is obtained as $\angle H_j(\omega) = 2\angle S(\omega)$ because $H_j(\omega)$ is composed of the frequency characteristics $Y_{\text{t}}(\omega)$ and $Y_{\text{r}}(\omega)$ of transmitting and receiving transducers, respectively. In the present study, the same transducer was used for transmitting and receiving [$Y_{\text{t}}(\omega) = Y_{\text{r}}(\omega) = Y(\omega)$].

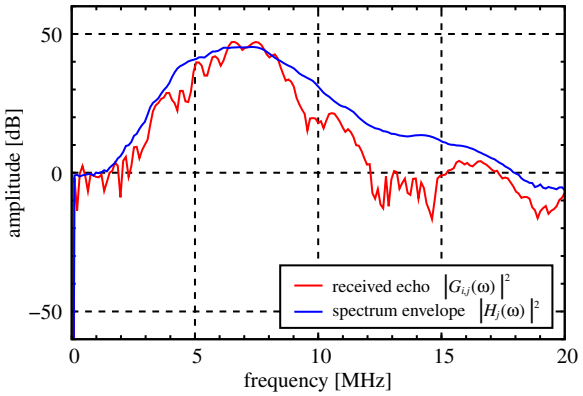

Fig. 5. (Color online) Spectrum envelope (corresponding to $|H_j(\omega)|$) obtained by averaging the power spectra of the received echoes $\{|G_{i,j}(\omega)|\}$ from a silicone plate with respect to beam position and the power spectrum of the received RF echo $|G_{i,j}(\omega)|$ at the lateral position of 15.0 mm ($i = 150$).

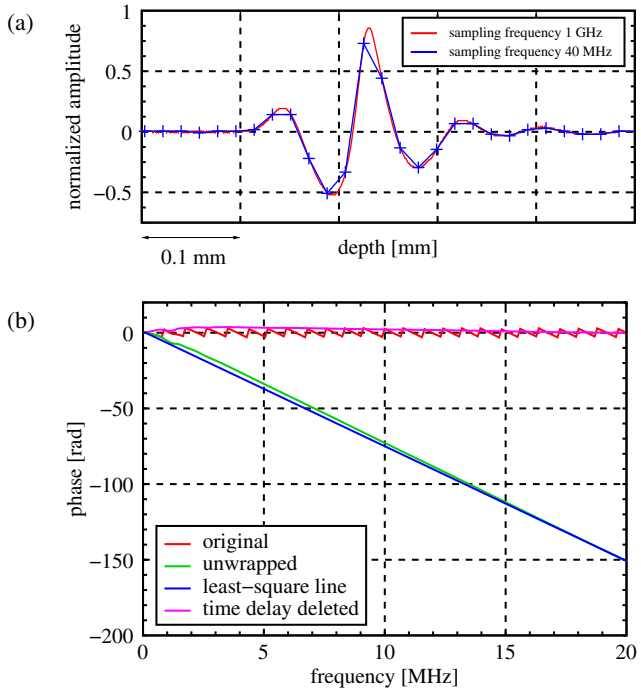

Fig. 6. (Color online) (a) Emitted ultrasonic pulse sampled at 1 GHz and same pulse downsampled to 40 MHz. (b) Phase spectra of the signal in (a).

An ultrasonic pulse received by a hydrophone (FORCE Technology MHA9-150) placed in a water tank is shown in Fig. 6(a). In the present study, modified ultrasonic diagnostic equipment (ALOKA SSD-6500 with a 10-MHz linear array probe) was used for transmitting and receiving ultrasonic pulses. The signal received by the hydrophone was sampled at 1 GHz using an oscilloscope (Tektronix TDS-2014). The signal acquired by the oscilloscope was downsampled to 40 MHz because the ultrasonic echo signal obtained by the SSD-6500 diagnostic equipment was sampled at 40 MHz. Figure 6(b) shows the phase spectrum $\angle S(\omega)$ of the signal received by the hydrophone. There is a constant slope in the entire phase spectrum owing to the time delay of ultrasonic propagation from the linear array to the hydrophone. The phase change due to the ultrasonic propagation is proportional to the frequency. Therefore, the constant slope was removed by estimating the regression line of the phase spectra using the least-squares method. Twice the residual phase was used as the phase $\angle H_j(\omega)$ of the transfer function.

2.3 Control parameter β used for weighting function

Section 2.1 described a method which estimates the SNR, $P_F(\omega)/P_N(\omega)$, using the MSCF. In addition, the relative magnitude of the weighting function $P_N(\omega)/P_F(\omega)$ to the transfer function $H_j(\omega)$ needs to be determined. The Wiener filter $M_j(\omega)$ behaves as an inverse filter $1/H_j(\omega)$ when the SNR is much larger than the magnitude of the transfer function $|H_j(\omega)|$. On the other hand, if the SNR is small, the Wiener filter $M_j(\omega)$ behaves as a matched filter. Methods using a real constant to control the contribution of the weighting function have been developed,[27,28] and methods in which the weighting function $P_N(\omega)/P_F(\omega)$ is controlled by multiplying by a control parameter β, which is called pseudo inverse filtering, have also been developed.[29–31] The former limits the effect of the Wiener filter $M_j(\omega)$ by assuming that the SNR is constant at every frequency. The latter realizes a wider bandwidth of the filter by controlling the effect of the weighting function $P_N(\omega)/P_F(\omega)$. A smaller control parameter β (≥ 0) is usually preferred in order to improve the spatial resolution at the expense of increased noise. In a conventional Wiener filter, $\beta = 1.0$. On the other hand, the filter works as an inverse filter at every frequency when β is low, corresponding to the assumption of a high SNR at all frequencies. In such a case, the noise in the frequency band away from the resonant frequency of a transducer tends to be amplified even though better spatial resolution is realized. Thus, the improvement of the spatial resolution was evaluated using the received echoes from a fine wire (13 μm in diameter), which corresponds to a point scatterer. A 10-MHz linear array probe was used, the sampling frequency of the ultrasonic RF echo was 40 MHz, and the frame rate was 30 Hz. The magnitudes of the transfer function $H_j(\omega)$ and weighting function $P_N(\omega)/P_F(\omega)$ were both normalized to limit control parameter β to between 0 and 1 as follows:

$$H_j(\omega)|_{\text{normalized}} = \frac{1}{\sqrt{\sum_{\omega=0}^{\omega_n} |H_j(\omega)|^2}} \cdot H_j(\omega), \tag{6}$$

$$\left.\frac{P_N(\omega)}{P_F(\omega)}\right|_{\text{normalized}} = \frac{1}{\sum_{\omega=0}^{\omega_n} \left(\frac{P_N(\omega)}{P_F(\omega)}\right)} \cdot \frac{P_N(\omega)}{P_F(\omega)}, \tag{7}$$

where ω_n is the Nyquist angular frequency. The spatial resolution (defined by the full width at half maximum) was evaluated by applying the Wiener filter $M_j(\omega)$ at different values of β to the echo from the fine wire, as shown in Fig. 7(a). The optimal control parameter β_{opt} was 0.01706 as shown in Fig. 7(a). As shown in Fig. 7(b), the duration of the received echo from a fine wire was shortened (the full width at half maximum was improved from 0.20 to 0.12 mm). Using this optimal control parameter β_{opt}, the proposed Wiener filter is defined as follows:

$$M_j(\omega) = \frac{H_j^*(\omega)|_{\text{normalized}}}{|H_j(\omega)|_{\text{normalized}}|^2 + \beta_{opt} \cdot \left.\frac{P_N(\omega)}{P_F(\omega)}\right|_{\text{normalized}}}. \tag{8}$$

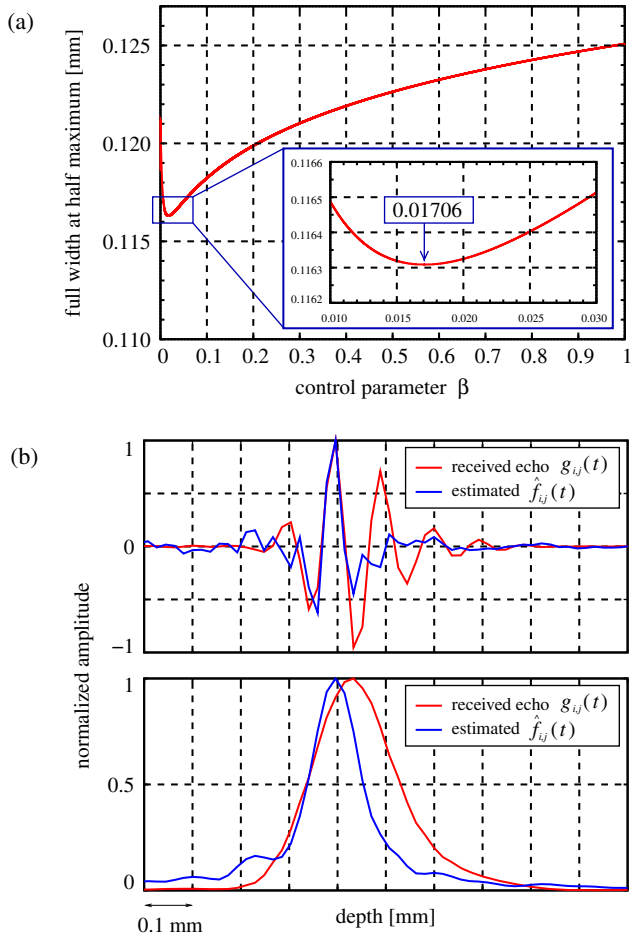

Fig. 7. (Color online) (a) Evaluation of the spatial resolution using the received RF echo from a fine wire (13 μm in diameter) for determining control parameter β of the weighting function $P_N(\omega)/P_F(\omega)$. (b) Received RF echo $g_{i,j}(t)$ from a fine wire (13 μm in diameter), the estimate $\hat{f}_{i,j}(t)$, and their envelopes obtained using the proposed Wiener filter $M_j(\omega)$ controlled by the optimal control parameter β_{opt}.

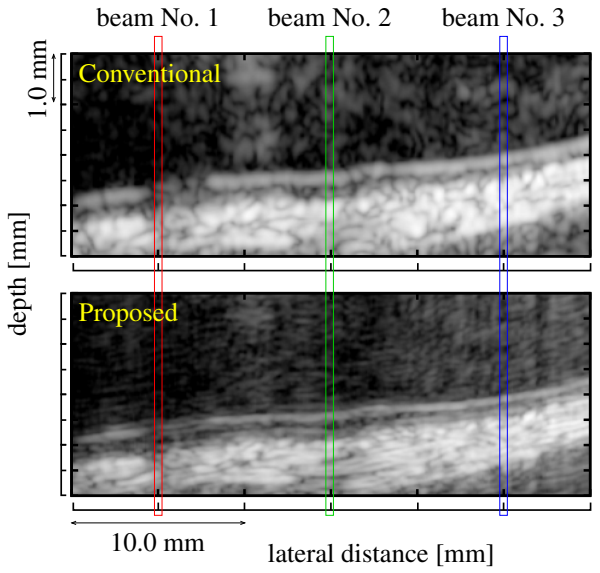

Fig. 8. (Color online) (a) Conventional B-mode image of a carotid artery of a posterior wall and (b) B-mode image obtained by applying proposed Wiener filter $M_j(\omega)$ with optimal control parameter $\beta_{opt} = 0.01706$.

3. Experimental Results and Discussion

Figure 8 shows a conventional B-mode image of a carotid artery of a 25-year-old healthy male and the B-mode image obtained by the proposed Wiener filter with the optimal control parameter β_{opt}, which was determined in the measurement of a fine wire as described in Sect. 2.3. As shown in Fig. 8, the noise in the intravascular lumen was reduced by the proposed Wiener filter $M_j(\omega)$. In addition, the brightnesses of the adventitia and intima in the posterior wall became distinct.

The power spectra of the original echo $g_{i,j}(t)$ and the estimate $\hat{f}_{i,j}(t)$ at 5.0, 15.0, and 25.0 mm in the lateral direction ($i = 50$, 150, and 250, corresponding to beam Nos. 1, 2, and 3 in Fig. 8, respectively), and the power spectra of the transfer function $H_j(\omega)$, weighting function $P_N(\omega)/P_F(\omega)$, and Wiener filter $M_j(\omega)$ ($j = 0$) are shown in Fig. 9. The power spectra of the estimates were broadened by the proposed Wiener filter as shown in Fig. 9. However, in the power spectrum of the weighting function in Fig. 9, the peak frequency of 3 MHz was lower than that of the nominal center frequency of 10 MHz. It is considered that the movement of the carotid artery degraded the coherency among signals, particularly in the high-frequency range, because the motion (corresponding to the time shift of the echo signal) leads to a larger phase shift at higher frequencies. Therefore, the SNR at low frequencies became larger than that at high frequencies. In future work, correction of the influence of the movement of a target in in vivo measurement needs to be investigated.

The received ultrasonic RF echoes $\{g_{i,j}(t)\}$ at 5.0, 15.0, and 25.0 mm in the lateral direction ($i = 50$, 150, and 250, respectively) and the estimates $\{\hat{f}_{i,j}(t)\}$ obtained using the proposed Wiener filter $M_j(\omega)$ are shown in Fig. 10(a), and the envelopes are shown in Fig. 10(b). In addition, as shown in Fig. 10(b), the lumen–intima boundary (LIB) and media–adventitia boundary (MAB) became distinct, and thus, it became easier to measure the IMT, especially in beams No. 2 and 3.

In the present study, the magnitude of the transfer function (corresponding to the PSF), $|H_j(\omega)|$, was determined using echoes in the whole measured region. Therefore, the performance of the proposed Wiener filter would be degraded if the frequency characteristics of echoes were changed by undesirable phenomena, such as frequency-dependent attenuation of the propagation medium. For measurement of the carotid artery, the above-mentioned method of designing the filter is effective because echoes from the media–adventitia interface of the arterial wall, which is the object of interest, are dominant in the region measured in the present study. However, in future work, the performance of the proposed filter should be improved by designing the filter region by region.

4. Conclusions

In this study, we proposed a method for improving the spatial resolution of an ultrasonic image, that is, broadening the frequency characteristics of the received echoes of an echo signal, using a Wiener filter. To determine an

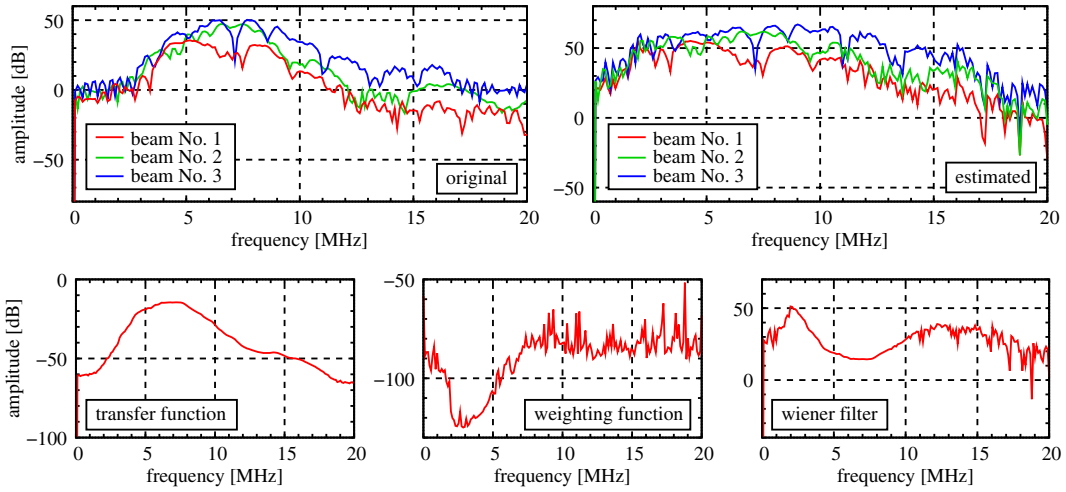

Fig. 9. (Color online) Power spectra of original echoes $\{g_{i,j}(t)\}$ and estimates $\{\hat{f}_{i,j}(t)\}$ at 5.0, 15.0, and 25.0 mm in the lateral direction ($i = 50$, 150, and 250, respectively), and the power spectra of the transfer function $H_j(\omega)$, weighting function $P_N(\omega)/P_F(\omega)$, and Wiener filter $M_j(\omega)$ ($j = 0$).

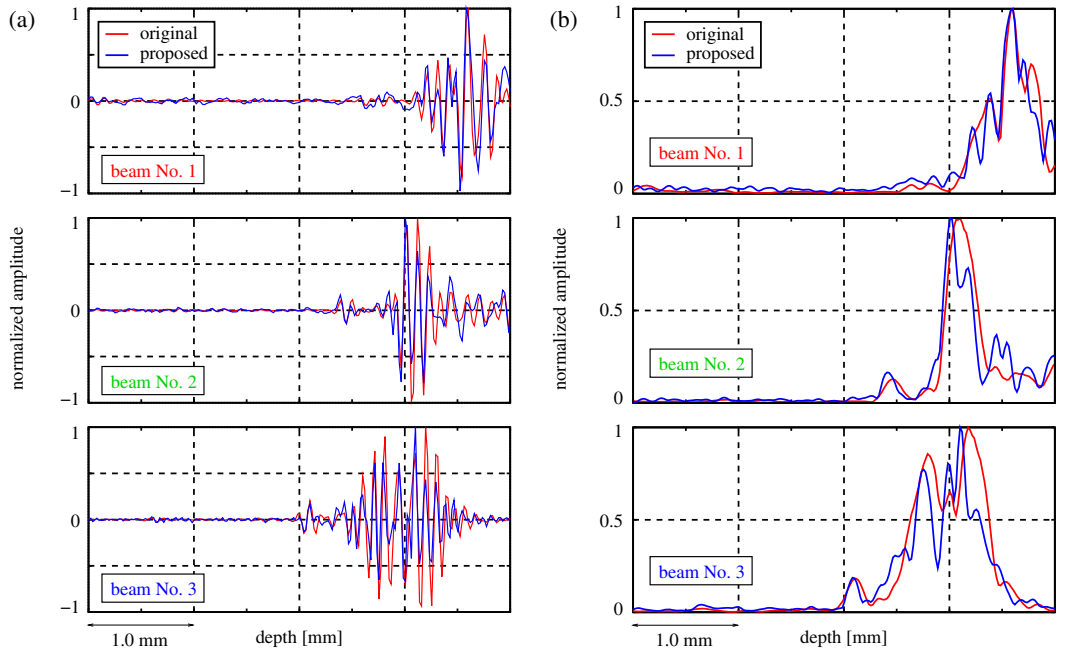

Fig. 10. (Color online) Received ultrasonic RF echoes $\{g_{i,j}(t)\}$ at 5.0, 15.0, and 25.0 mm in the lateral direction ($i = 50$, 150, and 250, respectively) and the estimates $\{\hat{f}_{i,j}(t)\}$, and their envelopes obtained using the proposed Wiener filter $M_j(\omega)$ ($j = 0$).

appropriate weighting function for the Wiener filter, the SNR was estimated using the magnitude-squared coherence function. In the proposed Wiener filter, the power of the transfer characteristic was obtained by averaging the power spectra of received echoes from an object of interest, each of which has many dips. The phase of the transfer characteristic was obtained from the phase of the ultrasonic pulse emitted from diagnostic equipment. Also, the optimal parameter controlling the effect of the weighting function was determined by evaluating the spatial resolution using the received echo from a fine wire. The proposed method was also applied to echoes from the carotid artery. The spatial resolution of the B-mode image was improved and the intima–media thickness of the posterior wall could be identified more easily.

1) E. Sho, M. Sho, T. M. Singh, H. Nanjo, M. Komatsu, C. Xu, H. Masuda, and C. K. Zarins: Exp. Mol. Pathol. **73** (2002) 142.
2) K. Kitamura, H. Hasegawa, and H. Kanai: Jpn. J. Appl. Phys. **51** (2012) 07GF08.
3) N. Ibrahim, H. Hasegawa, and H. Kanai: Jpn. J. Appl. Phys. **51** (2012) 07GF07.
4) C. Arihara, H. Hasegawa, and H. Kanai: Jpn. J. Appl. Phys. **45** (2006) 4727.
5) T. Kimura, H. Kanai, and N. Chubachi: IEICE Trans. Fundam. Electron. Commun. Comput. Sci. **E78-A** (1995) 1677.
6) S. Huber, M. Wagner, M. Medl, and H. Czembirek: Ultrasound Med. Biol. **28** (2002) 155.
7) M. Pernot, M. Tanter, J. Bercoff, K. R. Waters, and M. Fink: IEEE Trans. Ultrason. Ferroelectr. Freq. Control **51** (2004) 606.
8) J. R. Sanchez and M. L. Oelze: IEEE Trans. Ultrason. Ferroelectr. Freq. Control **56** (2009) 1327.
9) P. A. Magnin, O. T. von Ramm, and F. L. Thurstone: Ultrason. Imaging **4** (1982) 267.
10) G. E. Trahey, J. W. Allison, S. W. Smith, and O. T. von Ramm: Ultrason.

Imaging **8** (1986) 151.
11) I. Akiyama, N. Yoshizumi, and K. Nakamura: Proc. IEEE Ultrasonics Symp., 2009, p. 2712.
12) J. G. Abbott and F. L. Thurstone: Ultrason. Imaging **1** (1979) 303.
13) S. M. Gehlbach and F. G. Sommer: Ultrason. Imaging **9** (1987) 92.
14) H. E. Melton, Jr. and P. A. Magnin: Ultrason. Imaging **6** (1984) 159.
15) V. L. Newhouse, N. M. Bilgutay, J. Saniie, and E. S. Furgason: Ultrason. Imaging **20** (1982) 59.
16) F. L. Lizzi, M. E. Elbaum, and E. Feleppa: U.S. Patent 4561019 (1985).
17) N. Yoshizumi, S. Saito, D. Koyama, K. Nakamura, A. Ohya, and I. Akiyama: J. Med. Ultrason. **36** (2009) 53.
18) A. Rosenfeld and A. C. Kak: *Dijitaru Gazo Shori* (Digital Image Processing) (Kindai Kagaku, Tokyo, 1978) [in Japanese].
19) W. K. Pratt: *Digital Image Processing* (Wiley, New York, 1978).
20) H. C. Andrew and B. R. Hunt: *Digital Image Restoration* (Prentice Hall, Upper Saddle River, NJ, 1997).
21) M. Saito: *Dijitaru Gazo Shori* (Digital Image Processing) (Tokai University Press, Hiratsuka, 1986).
22) J. Jan: *Medical Image Processing, Reconstruction and Restoration: Concepts and Methods* (CRC Press, Boca Raton, FL, 2005).
23) H. Kanai: *Oto to Shindo no Supekutoru Kaiseki* (Spectrum Analysis of Sound and Vibration) (Corona, Tokyo, 2008) [in Japanese].
24) T. Fukushima, H. Hasegawa, and H. Kanai: Jpn. J. Appl. Phys. **50** (2011) 07HF02.
25) T. Taxt and R. Jiřík: IEEE Trans. Ultrason. Ferroelectr. Freq. Control **51** (2004) 163.
26) D. Iracà, L. Landini, and L. Verrazzani: IEEE Trans. Ultrason. Ferroelectr. Freq. Control **36** (1989) 216.
27) W. Yeoh and C. Zhang: IEEE Trans. Biomed. Eng. **53** (2006) 2001.
28) S. Sin and C. Chen: IEEE Trans. Image Process. **1** (1992) 3.
29) S. Måsøy, T. F. Johansen, and B. Angelsen: J. Acoust. Soc. Am. **113** (2003) 2009.
30) S. Hantscher, A. Reisenzahn, and C. G. Diskus: IET Rader Sonar Navig. **2** (2008) 315.
31) J. R. Fienup, D. K. Griffith, L. Harrington, A. M. Kowalczyk, J. J. Miller, and J. A. Mooney: Proc. SPIE **4792** (2002) 1.